Band structure, photoelectron spectroscopy, and transport properties of $SnTaS_2$

J. Dijkstra,* E. A. Broekhuizen, C. F. van Bruggen, and C. Haas
Laboratory of Inorganic Chemistry, Materials Science Centre of the University, Nijenborgh 16, 9747 AG Groningen, The Netherlands

R. A. de Groot
Research Institute for Materials, Faculty of Science, Toernooiveld, 6525 ED Nijmegen, The Netherlands

H. P. van der Meulen
Physical Laboratory, University of Amsterdam, Valckenierstraat 65, 1018 XE Amsterdam, The Netherlands
(Received 30 November 1988; revised manuscript received 1 September 1989)

We present band-structure calculations of $SnTaS_2$, an intercalation compound in which the Sn atoms have a very uncommon linear coordination by two S atoms and an unusual formal valency Sn^{1+}. The Sn $5p_x$ and $5p_y$ states show strong metal-metal bonding in the intercalant planes and the Fermi level is crossed by a very wide band composed of these Sn $5p_xp_y$ states. Angle-resolved photoelectron spectra are in agreement with the calculated band structure. $SnTaS_2$ is metallic as is reflected in the measured transport properties (resistivity, Hall effect, thermoelectric power). Low-temperature specific-heat measurements show an anomaly due to superconductivity below 2.8 K. The Sn 4*d* core levels, measured with photoelectron spectroscopy, show a splitting of 1 eV, indicating the presence of two different types of Sn atoms. This could be due to a valence disproportionation $2Sn^+ \rightarrow Sn^0 + Sn^{2+}$ and rapid valence fluctuations between Sn^0 and Sn^{2+}.

I. INTRODUCTION

The layered transition-metal dichalcogenides easily allow the intercalation of a great variety of metal atoms. The structures and physical properties of these intercalation compounds have been studied in detail, using many different experimental techniques. In review articles[1-4] a great variety of phenomena occurring in intercalates, as metal-semiconductor transitions, ionic conduction, charge-density waves and order-disorder phenomena, are discussed.

The intercalated atoms occupy sites in the van der Waals gap between the sandwich layers of the host compound. For intercalated transition-metal atoms these are the octahedral sites in the van der Waals gap. Intercalation of alkali metals leads to the occupation of octahedral or tetrahedral-prismatic sites in the van der Waals gap. Intercalated Ag and Cu atoms occupy octahedral or tetrahedral sites in the van der Waals gap. In all these cases the intercalated metal atoms donate electrons to the lowest unoccupied or partly occupied band of the host compound, in order to reach the "normal" valency expected for a metal atom in a chalcogen lattice (i.e., A^+ for the alkali atoms, Ag^+, Cu^+, and M^{2+} or M^{3+} for the 3*d* transition-metal atoms). For the compounds TX_2 (T=Nb,Ta; X=S,Se) with the 2*H* structure, in which T has a trigonal-prismatic coordination by X atoms, this lowest partly occupied band is the so-called "d_{z^2}" band, which is occupied by one electron per formula unit, and can contain at most two electrons per formula unit. The intercalation and associated electron donation can generally proceed until this d_{z^2} band is fully occupied. This sets an upper limit for the concentration of the intercalated atoms.

It is also possible to intercalate the post-transition metals M=Ga,In,Sn,Pb,Bi into TaS_2, $TaSe_2$, NbS_2, and $NbSe_2$.[1,5] The resulting intercalation compounds M_xTX_2 are of two distinct types: the fully intercalated compounds with $x=1$ and compounds with $x \simeq \frac{1}{3}, \frac{1}{4}$. In the latter type the intercalated atoms occupy octahedral sites in the van der Waals gap.

In this paper we will concentrate on the fully intercalated compounds of post-transition metals and in particular on $SnTaS_2$. This compound shows some very interesting and unusual features. In the first place the Sn atoms do not occupy an octahedral, tetrahedral, or trigonal-prismatic site in the van der Waals gap, as observed in all other intercalation compounds. In $SnTaS_2$ the intercalated Sn atoms are linearly coordinated by two sulfur atoms and the Sn atoms form hexagonal two-dimensional sheets in the van der Waals gap of the TaS_2 host compound.[6] Secondly, the Sn atoms in $SnTaS_2$ have an uncommon formal valency of Sn^{1+} ($5s^2, 5p^1$); this valency is deduced if it is assumed that intercalation is associated with electron donation to the Ta d_{z^2} band until this band is fully occupied. $SnTaS_2$ is a metallic compound,[7] and shows superconducting behavior at low temperature.[5] Some features of Sn 3*d* core photoelectron spectroscopy have been interpreted as evidence for the presence of valence fluctuations in $SnTaS_2$.[8]

We present in this paper calculations of the band structure of $SnTaS_2$ and some related compounds, using the

augmented-spherical-wave (ASW) method. The calculations support the already mentioned unusual valency of Sn in $SnTaS_2$. We find some important differences with recently published band-structure calculations of $SnTaS_2$ with the atomic-sphere-approximation–linear-muffin-tin-orbital (ASA-LMTO) method.[9] The calculated band structure is compared with new angle-resolved and photon-energy-dependent photoemission studies of the valence band. We also report measurements of several physical properties, such as electrical conductivity, Hall effect, thermoelectric power, and low-temperature specific heat. Finally, we present new Sn 4*d* photoemission data, in an attempt to find evidence for the valence fluctuations suggested previously.

II. PREPARATION AND CRYSTAL STRUCTURES

Polycrystalline $SnTaS_2$ and $Sn_{1/3}TaS_2$ were obtained by heating the elements for one week at 800–900 °C and, after repowdering, for another week at 800–900 °C. The largest single crystals of $SnTaS_2$ were obtained by the following gas transport reaction at temperatures of 700–900 °C, lasting three weeks:

$$Sn_{1/3}TaS_2(\text{powder}) + \tfrac{2}{3}Sn \rightarrow SnTaS_2 \ ;$$

where Cl_2 was used as transport gas. Crystals were formed at the low-temperature side. Smaller single crystals were obtained by a gas transport reaction with $SnTaS_2$ powder as starting material.

The crystal structure and lattice parameters were obtained by x-ray diffraction. Stoichiometry was determined by chemical analysis.

The crystal structure of the host compound $2H$-TaS_2, with two slabs per unit cell, is shown in Fig. 1(a) and the (110) section of the unit cell in Fig. 1(b). For $2H$-TaS_2 the intercalant positions in Fig. 1(b) are empty. The Ta atoms are in a trigonal-prismatic coordination by S.

Eppinga and Wiegers[6] made an extensive study of the crystal structures occurring in post-transition-metal intercalates of Ta and Nb dichalcogenides. For fully intercalated ($x = 1$) compounds several classes can be distinguished.

(a) The $2s$-$SnTaS_2$ structure [see Fig. 1(c)]. There are two formula units and two slabs per unit cell. This structure is found for $SnTaS_2$, $SnNbS_2$, $PbTaS_2$, and $PbNbS_2$. The atoms are in the following special positions of the space group $P6_3/mmc$ [see *International Tables of Crystallography* (Reidel, Dordrecht, 1983), Vol. A, Tab. 194]:

$2M$ in $2a$: $(0,0,0),(0,0,\frac{1}{2})$,

2 Ta in $2c$: $\pm(\frac{1}{3},\frac{2}{3},\frac{1}{4})$,

4 S in $4e$: $\pm(0,0,z)$, $\pm(0,0,z+\frac{1}{2})$ with $z \approx 0.33$.

Ta atoms are in a trigonal-prismatic coordination by S, but the stacking of the TaS_2 slabs has changed as compared to $2H$-TaS_2. The intercalant atoms M are linearly coordinated by S and form two-dimensional hexagonal sheets in which they have six neighbors at a distance equal to the a axis. The c axis increases with about 2.7 Å per slab, as compared to $2H$-TaS_2.

(b) The $1s$-$MTaS_2$ structure [Fig. 1(d)]. In this structure there is only one slab per unit cell. This structure is found for $PbTaSe_2$, $InTaS_2$, and $SnNbSe_2$.[6] The structure can be described in the space group $P\bar{6}m2$ (see Tab. 187 in the above mentioned *International Tables of Crystallography*) with the atoms in the following positions:

1 M in $1a$: $(0,0,0)$,

1 Ta in $1d$: $(\frac{1}{3},\frac{2}{3},\frac{1}{2})$,

2 S in $2g$: $\pm(0,0,z)$ with $z \approx 0.32$.

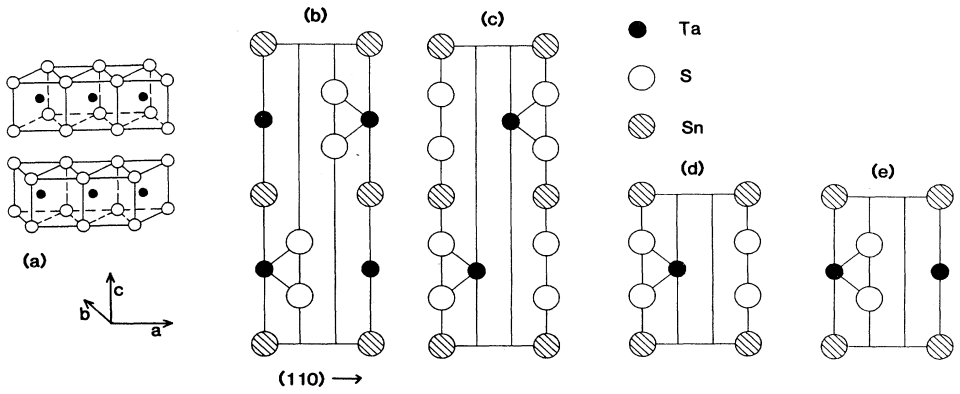

FIG. 1. (a) Crystal structure of $2H$-TaS_2. (b) (110) section of the unit cell of $2H$-TaS_2, with the octahedral intercalant positions. (c) (110) section of the unit cell of $2s$-$MTaS_2$. (d) (110) section of the unit cell of $1s$-$MTaS_2$. (e) (110) section of the unit cell of M_xTaS_2; M atoms are trigonal prismatically coordinated.

The only difference with the above-mentioned 2*s*-MTaS$_2$ structure is the stacking of the TaS$_2$ layers; the Ta atoms of different slabs are now right above each other along c axis. Because of the large Ta-Ta distance along the c axis this change has little influence on the electronic structure as will be shown in the following paragraph. The c axis increase is about 2.7 Å per slab as in the 2*s* structure.

(c) The M_xTaS$_2$ structure [Fig. 1(e)]. In this case there is one formula unit and one slab per unit cell. This structure is observed for InNbS$_2$ and InTaSe$_2$.[6] Both the post-transition metal M and the Ta atom are in trigonal-prismatic coordination by S. The change in the c axis ($\sim$1.9 Å per slab) is appreciably smaller than for the 2*s* and 1*s* structure.

SnTaS$_2$ crystallizes in the 2*s* structure, described under (a). Band-structure calculations have been performed for SnTaS$_2$ with the 2*s* structure and the 1*s* structure.

The z parameter of the positions of the sulfur atoms in these structures have not been determined very accurately. Comparison of the structural parameters of many TaS$_2$ intercalates shows that distances within the TaS$_2$ slabs are approximately equal for intercalation compounds with different metal atoms. So in our definitive calculations we used z values corresponding to Ta-S distances of about 2.48 Å and intrasandwich S-S distances along c of 3.14 Å.

III. BAND-STRUCTURE CALCULATIONS

A. Details of the calculations

Self-consistent calculations of the electronic band structure were performed using the augmented-spherical-wave[10] method. Exchange and correlation were treated within the local-spin-density approximation.[11] Scalar relativistic effects were included.[12]

The basis functions were composed of 5*s*, 5*p*, and 5*d* functions on Sn; 6*s*, 6*p*, and 5*d* on Ta; and 3*s*, 3*p*, and 3*d* on S. 4*f* functions on Sn and S and 5*f* functions on Ta were included in the internal summation of the three-center contributions to the matrix elements, what can be regarded as treating these *f* states as a perturbation.

When a crystal structure is not very densely packed—as is the case in layered compounds with a van der Waals gap or intercalation compounds with a linear coordination of the intercalant atoms—it is sometimes necessary to include empty spheres in the calculation. For 1*s*-SnTaS$_2$ two empty spheres at the (2*i*) positions between the Sn and S layers are included. For 2*s*-SnTaS$_2$ empty spheres at the equivalent positions were included. Lattice constants and Wigner-Seitz sphere radii used in the band-structure calculations are tabulated in Table I.

TABLE I. Lattice constants a and c and Wigner-Seitz sphere radii r_i used in the band-structure calculations. All values are in Å.

	2H-TaS$_2$	1*s*-SnTaS$_2$	PbTaS$_2$	GeTaS$_2$
a	3.316	3.307	3.326	3.310
c	12.07	8.72	8.85	8.56
c/a	3.64	2.637	2.661	2.587
r_{Ta}	1.373	1.270	1.270	1.270
r_S	1.772	1.654	1.675	1.628
$r_{intercalant}$		1.654	1.675	1.638
$r_{empty\ sphere}$		1.270	1.270	1.270

B. 2H-TaS$_2$

For the interpretation of the electronic structure of intercalates of 2H-TaS$_2$ a comparison with a band-structure calculation—by the same method—of the host lattice 2H-TaS$_2$ is necessary. The input parameters of the calculation of 2H-TaS$_2$ are given in Table I. For 2H-TaS$_2$ no empty spheres were included since it was shown that in the ASW approximation for a comparable layer compound (MoS$_2$) inclusion of empty spheres leads to essentially the same result as a calculation without empty spheres.[13] In Fig. 2 the band structure of 2H-TaS$_2$ along symmetry lines in the Brillouin zone is shown. Information about the wave-function character of the bands can be obtained from the total and partial density of states (DOS) in Fig. 3.

The lowest band at 14 eV below the Fermi level consists of S 3*s* states. The 6-eV wide band from -1.5 to -7.5 eV is mainly composed of S 3*p* states. Above this band lies the so-called Ta 5d_{z^2} band, which is energetically separated from the other Ta 5*d* states. The Ta 5d_{z^2} band, with a width of 1.26 eV, can contain two electrons, but is only half-filled. This band is of great importance for metal intercalation, since the electrons donated to the TaS$_2$ layers by the intercalant atoms fill up this band. The fact that there is only room for one extra electron per formula unit determines the upper limit of the concentration of intercalant atoms.

From the partial DOS (Fig. 3) it is clear that there is a strong covalency between the S 3*p* states and the Ta 5*d* states. This hybridization is also the reason for the splitting off of the Ta 5d_{z^2} band from the rest of the Ta 5*d* manifold. The formation of the d_{z^2} band, which also con-

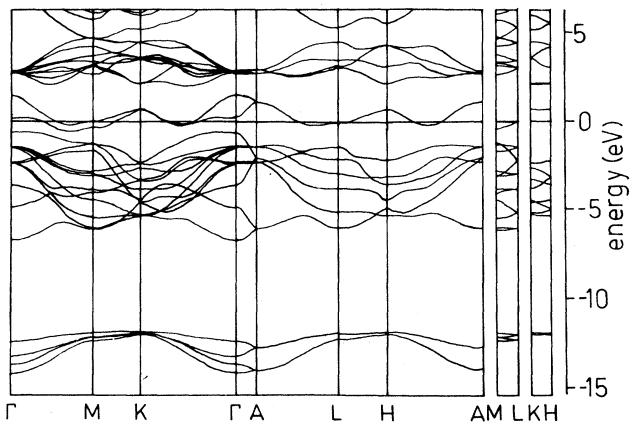

FIG. 2. Energy band structure of 2H-TaS$_2$.

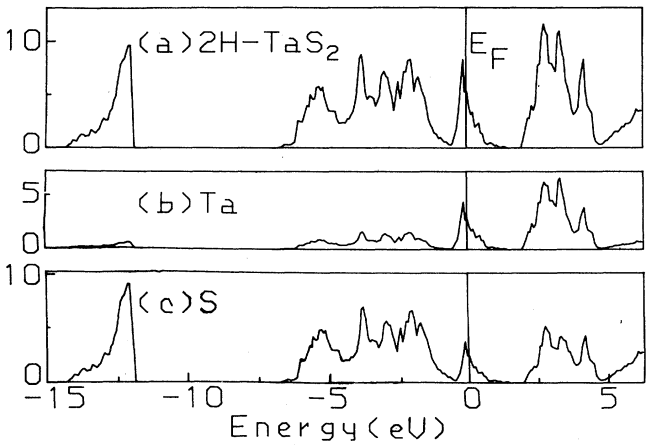

FIG. 3. Density of states (DOS) of $2H$-TaS_2. (a) Total DOS. (b) Partial Ta DOS. (c) Partial S DOS. Units: states eV^{-1} (formula unit)$^{-1}$.

tains considerable Ta $5d_{xy}$ and $5d_{x^2-y^2}$ and sulfur character away from Γ, stabilizes the trigonal-prismatic coordination of Ta (d^1) by the sulfur atoms.[14]

Our calculated band structure is in reasonable agreement with the ASA-LMTO results.[9] The older APW calculation[15] gives the same dispersions, but a different Ta $5d$–S $3p$ gap, probably due to the fact that this calculation is not self-consistent.

When using spherically symmetric potentials in the self-consistent loop, as in the ASW method, the polarization of the S atoms due to their asymmetric coordination by Ta is not taken into account self-consistently. Band-structure calculations and photoemission results of comparable layered compounds such as $MoSe_2$, $TiSe_2$, and $1T$-$TaSe_2$ are in better agreement with each other, when in the calculation the chalcogens are slightly shifted towards the metal atoms—crudely simulating the anion polarization.[16] For $2H$-TaS_2 and its intercalates the measured structural data were used as input for the calculations, without trying to simulate the anion polarization, which seems justified by the fact that this correction is small for $1T$-$TaSe_2$.[16]

In our band structure there is a small overlap between the Ta d_{z^2} band and the top of the S $3p$ band, which is situated between Γ and M. The calculated DOS shows the same Ta d–S p peak-to-peak splitting as was measured by angle integrated ultraviolet photoemission spectroscopy (UPS).[17] The calculated overall bandwidth from the lowest S $3p$ band to the Fermi level is 6.8 eV. The above-mentioned UPS study gives a value of 6.5 eV.

C. 2*s*- and 1*s*-$SnTaS_2$

We now turn to the electronic structure calculations of $SnTaS_2$, which crystallizes in the $2s$ structure [Fig. 1(c)] with a z parameter of 0.32.[18] Calculations were performed for $2s$-$SnTaS_2$ and $1s$-$SnTaS_2$. The Brillouin zone of the $1s$ structure is twice as large as that of the $2s$ structure; it is doubled in the c direction. The number of energy bands is halved. Comparison of the results of band-structure calculations for both structures shows that the different stacking of the slabs hardly makes any difference. The eigenvalues of $1s$-$SnTaS_2$ in Γ and A, for example, are within 0.06 eV the same as the eigenvalues of $2s$-$SnTaS_2$ in Γ. (The halving of the crystallographic unit cell in the c direction leads to folding the symmetry point Γ of the $2s$ Brillouin zone onto Γ and A of the $1s$ Brillouin zone.) Consequently all the important aspects of the electronic structure show up in the calculation of $1s$-$SnTaS_2$. Therefore only the band structure of $1s$-$SnTaS_2$ is shown.

Band-structure calculations of $1s$-$SnTaS_2$ were performed with the addition of two empty spheres at the ($2i$) positions, in between the Sn and the S layers. Table I gives the input parameters of the calculation. In Fig. 4 the electron energy bands are shown. The wave-function character of different bands can be obtained from the total DOS [Fig. 5(a)] and the partial DOS [Figs. 5(b)–5(d)].

The lowest bands around 15 eV below the Fermi level with a width of 2 eV are almost completely of S $3s$ origin. The *seven* bands positioned between -2 and -9 eV below the Fermi energy E_F are of S $3p$ and Sn $5s$ origin. The Sn $5s$ states are very dispersive, giving a low partial DOS. Both the top in H and bottom in Γ (see Fig. 4) of this set of seven bands have mainly Sn $5s$ character. The Sn $5s$ states are mixed with the S $3p$ bands, mostly with the $3p_z$ states in the direction of the linear S-Sn-S array. The width of the S $3p$ band, with a much higher partial density of states than the Sn $5s$, is 5.4 eV, about the same value as found for $2H$-TaS_2.

Just below the Fermi level lies the Ta $5d_{z^2}$ band, which is completely filled in $SnTaS_2$. There has been a transfer of about one electron from Sn to the Ta $5d_{z^2}$ band. The rest of the Ta $5d$ manifold is situated above E_F. The Ta and S contributions to the DOS closely resemble the DOS of $2H$-TaS_2. The Ta $5d$–S $3p$ gap is slightly increased as

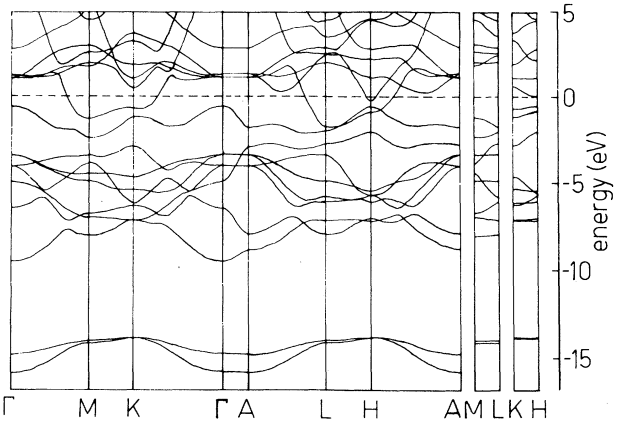

FIG. 4. Energy band structure of $1s$-$SnTaS_2$.

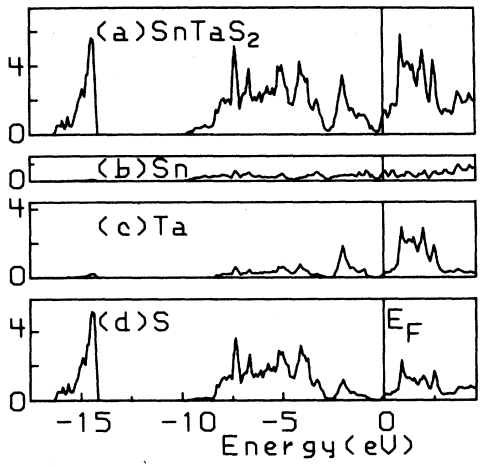

FIG. 5. Density of states of 1*s*-$SnTaS_2$. (a) Total DOS. (b) Partial Sn DOS. (c) Partial Ta DOS. (d) Partial S DOS. Units: states eV^{-1} (formula unit)$^{-1}$.

compared to 2*H*-TaS_2. The width of various bands is the same within 0.3 eV for the intercalate and the host compound. This equivalence is a consequence of the fact that the host band structure is mainly determined by the interactions within one TaS_2 sandwich and that elongation of the *c* axis due to intercalation has little influence. Further the Sn-TaS_2 interaction is not so strong that it causes large changes in the TaS_2 partial DOS.

The Sn 5*p* states are partly filled. The Sn $5p_z$-derived band—with lowest energy 3 eV above E_F at Γ—is empty. However, in the linear coordination of Sn by S the Sn $5p_z$ state hybridizes with the S $3p_z$ states, pushing the latter further down in energy, resulting in some Sn—S bonding. The Sn $5p_xp_y$ states form a 10.9-eV-wide band with its top in Γ and *A*, far above E_F. The bottom of this dispersive band is located in *L* at 2.5 eV below the Fermi level. The large bandwidth is a consequence of the overlap of the Sn $5p_xp_y$ states in the plane of the intercalated atoms, where the Sn-Sn distance is determined by the TaS_2 lattice parameter of 3.31 Å. This distance is not much larger than the Sn-Sn distance in α-Sn (3.02 and 3.18 Å). The very pronounced two-dimensional character of the Sn $5p_xp_y$ band is illustrated by the fact that it has little dispersion in the *z* direction.

To check the origin of the Sn $5p_xp_y$ band we have calculated the energy bands of a single hexagonal layer of (Sn) atoms with only 5*p* states, using a simple tight-binding model. Only σ overlap of the *p* states is included. In this approximation the p_z states have no dispersion (they lie at a constant energy $E/t=0$) and are therefore not shown. The calculated DOS and the dispersion of the bands are shown in Figs. 6(a) and 6(b), respectively. Good agreement between the tight-binding calculation [Fig. 6(b)] and the ASW calculation [Fig. 6(c)] is obtained when the center of mass of the p_xp_y band is 3.26 eV above the Fermi level and the overlap parameter $t(pp\sigma)=1.9$ eV.

The Fermi level is crossed by the very wide Sn $5p_xp_y$ band, while around *H* a second (Ta *d*) band crosses E_F. The density of states at the Fermi level $N(E_F)=1.0$ states eV^{-1} $(SnTaS_2)^{-1}$.

From the calculated electronic structure the Fermi sur-

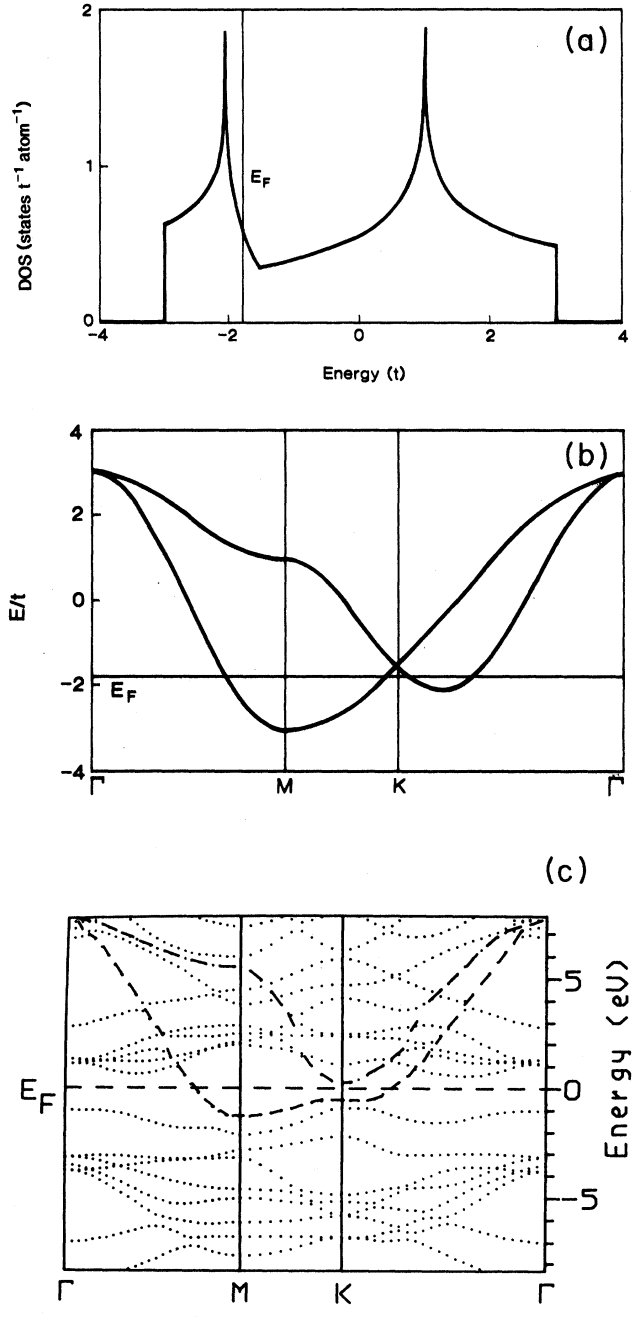

FIG. 6. The calculated Sn $5p_xp_y$ band. (a) Tight-binding method: density of states. (b) Tight-binding method: energy-dispersion curves along Γ*MK*Γ. (c) ASW method; dotted and dashed curves are ASW calculated energy bands. The dashed curves are bands with mainly Sn $5p_xp_y$ character.

faces of $SnTaS_2$ are constructed. The Ta $5d$ band gives rise to small electron pockets around H. The cross section of the Fermi surface of the Sn $5p_xp_y$ band with the central ΓMK plane of the Brillouin zone is shown in Fig. 7. The value of the component of the Fermi wave vector parallel to the layers changes by less than 1% when the third component of **k** is varied along the z direction. So the Fermi surface of $SnTaS_2$ consists of rosette-shaped parallel rods along the c direction. This confirms the two-dimensional character of the conduction electrons in the Sn $5p_xp_y$ band. The Sn $5p_xp_y$ Fermi surface is hole-like, since the slope of the energy band $E(k)$ crossing the Fermi level is negative and the states enclosed by the Fermi surface are empty.

The Sn $5p_xp_y$ band is about $\frac{1}{4}$ filled with one electron per Sn atom; the formal valency of Sn in this compound is thus 1^+ ($5s^25p^1$), while the usual valencies for Sn are zero for Sn metal and 2^+ and 4^+ in compounds like SnS, SnS_2, etc. The electron in the broad Sn $5p_xp_y$ band gives a stabilization energy of about 5.45 eV, equal to half the bandwidth, as compared to the case of negligible Sn-Sn interaction.

The band structure of $2s$-$SnTaS_2$, calculated by the ASA-LMTO method,[9] shows resemblance with our results. The most remarkable difference is the width and position of the intercalant p_xp_y band. Guo and Liang[9] find for $SnTaS_2$ and $PbTaS_2$ a width of the p_xp_y band of 8 and 7 eV, respectively, while our calculation gives 10.9 and 11.6 eV, respectively. Their intercalant p_z states lie much closer to E_F than in our calculation. Probably these differences originate from the difference in the chosen sphere radii. Due to the very open and anisotropic crystal structure it is necessary to include empty spheres in the calculation. A calculation without empty spheres necessarily leads to a strong overlap of the spheres, especially in the direction of the linear S-Sn-S array, which gives erroneous results. It is remarkable that Guo and Liang[9] do include empty spheres in the van der Waals gap in the calculation of $2H$-TaS_2, but do not do so for the larger empty spaces present in $2s$-$SnTaS_2$.

It is difficult to establish quantitatively why $SnTaS_2$ prefers the linear coordination above the other possibilities. Comparison of total-energy differences of nondense packed structures for systems with different volumes per unit cell is beyond the precision of the calculations. We can, however make some remarks about the relative stability of these intercalation compounds.

The stabilizing factors for post-transition-metal-intercalates are as follows.

(1) The electron transfer from the intercalant p states to the Ta d_{z^2} band. In $SnTaS_2$ one electron per formula unit is transferred, giving a completely filled d_{z^2} band.

(2) The hybridization of the intercalant p states with the S $3p$ band. In the linearly coordinated compounds mainly p_z states are involved. The interaction of the intercalant s states with the S $3p$ bands does not lead to a net bonding effect, since these s states are completely filled.

(3) The metal-metal interactions in the two-dimensional intercalant layers give a very wide p_xp_y band. In $SnTaS_2$ this band is occupied by one electron per Sn, giving an extra stabilization energy of about half the bandwidth. In the structures with linearly coordinated intercalant atoms the intercalant p_xp_y band has little interaction with the host bands and has the largest intercalant p bandwidth. Apparently this effect is more important than the energy that can be gained by increasing the Sn-S covalency, when the coordination of the intercalant atom is changed.

The first two arguments apply to all post-transition metal intercalates, while the third applies only to the fully intercalated ($x=1$) compounds.

We have also performed calculations for fictive, fully intercalated $SnTaS_2$ with the Sn atoms in other coordinations[19] (octahedral and tetrahedral) by the sulfur atoms and shorter Sn-Ta distances. Stronger Sn-Ta interactions are found than in the $2s$ and $1s$ structures. These Ta-Sn interactions disturb the formation of the two-dimensional Sn $5p_xp_y$ band, while also considerable differences, between intercalated and nonintercalated structures, in the Ta d bands are observed. So, the rigid-band model is no longer a good approximation, when intercalant-host interactions are increased.

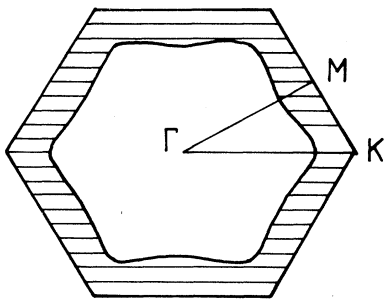

FIG. 7. Cross section of the Fermi surface of the Sn $5p_x5p_y$ band of $1s$-$SnTaS_2$ with the ΓMK plane.

D. $PbTaS_2$ and $GeTaS_2$

We have also calculated the electronic structure of the isoelectronic compounds $PbTaS_2$ and $GeTaS_2$ in the $1s$ structure. $PbTaS_2$ closely resembles $SnTaS_2$ in its properties, but $GeTaS_2$ does not exist.[5] For the nonexisting $GeTaS_2$ we have assumed the length of the a axis to be the same as in $Ge_{1/3}TaS_2$ (Ref. 5) and we have chosen the length of the c axis so that the internal pressure of the converged calculation was zero. The structure and input data of the calculations are given in Table I.

The calculated electron energy bands are shown in Fig. 8 and the density of states in Fig. 9. The width of the post-transition-metal s band increases in the series Ge-Sn-Pb. The most important difference however is found in the two-dimensional intercalant p_xp_y band. This band also increases in width in the series Ge-Sn-Pb (8.8-10.9-11.6 eV), as a consequence of the fact that the metal-

metal distances in the *ab* plane are approximately the same in all three compounds (3.31 Å, the *a* axis of TaS_2), while the atomic radii increase in the series Ge-Sn-Pb. As a consequence there is a smaller overlap between the in-plane Ge $4p_xp_y$ functions than between the spatially more extended Sn $5p_xp_y$ and Pb $6p_xp_y$ states. The decrease of the p_xp_y bandwidth reduces the energy gain by band formation by about 1.05 eV [=(10.9–8.8)/2] in $GeTaS_2$ with respect to $SnTaS_2$. This is one of the reasons for the nonexistence of $GeTaS_2$.

The values of the density of states at the Fermi level are 0.7 states eV^{-1} $(PbTaS_2)^{-1}$ and 0.6 states eV^{-1} $(GeTaS_2)^{-1}$. These values are smaller than in the case of $SnTaS_2$, because for both $GeTaS_2$ and $PbTaS_2$ the Fermi level is only crossed by the intercalant p_xp_y bands, but not by the Ta 5*d* band.

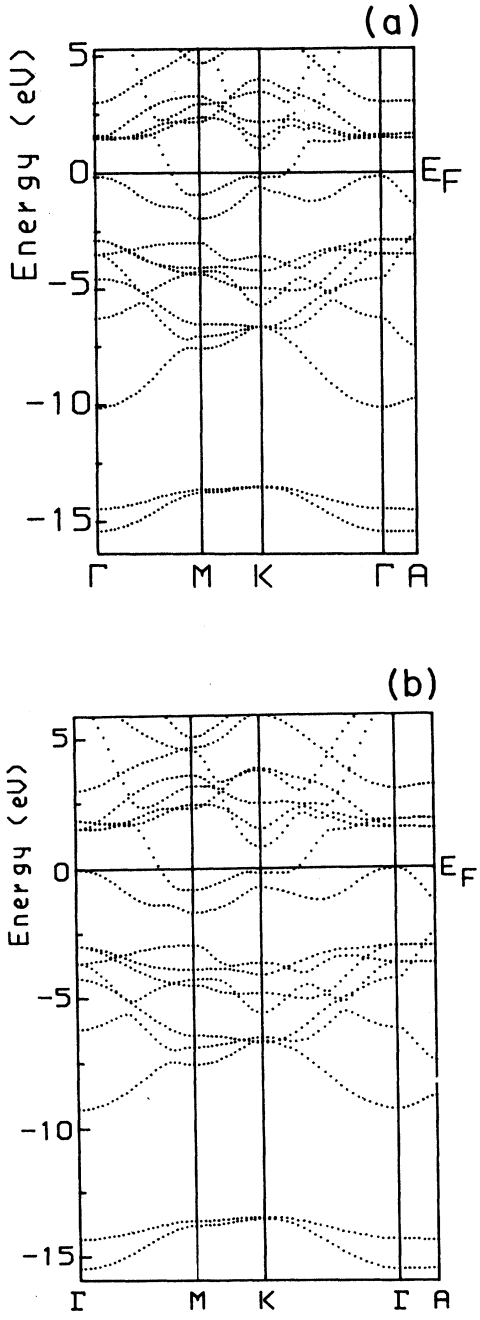

FIG. 8. Energy band structure of (a) 1*s*-$PbTaS_2$ and (b) 1*s*-$GeTaS_2$.

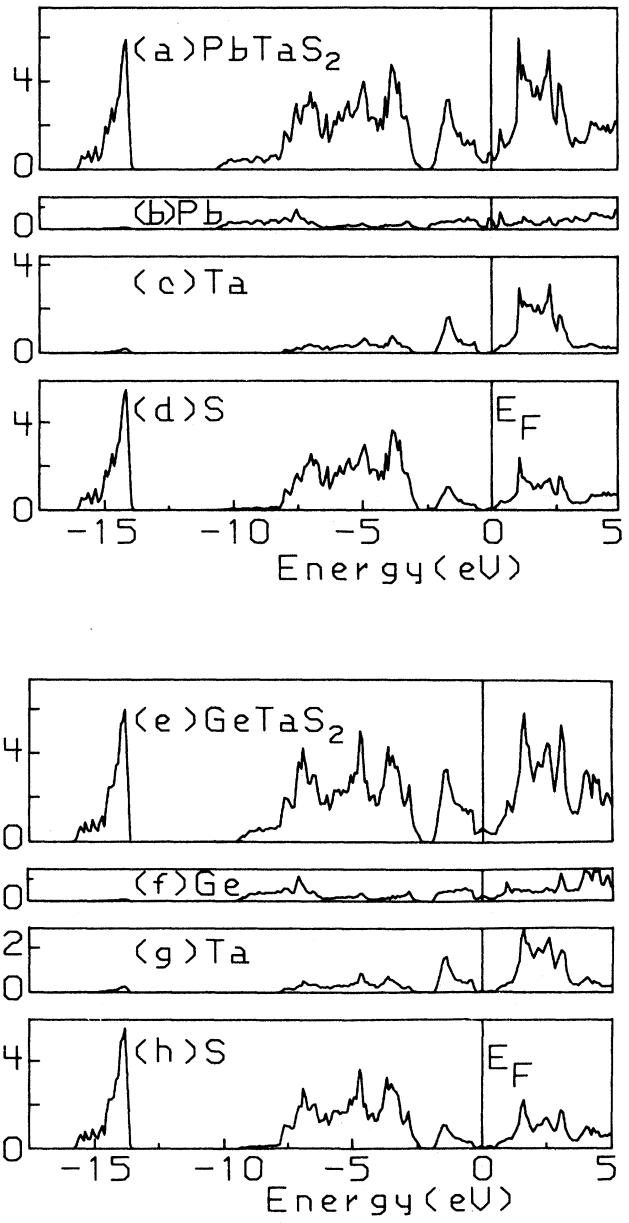

FIG. 9. Total and partial density of states of 1*s*-$PbTaS_2$ [(a)–(d)] and 1*s*-$GeTaS_2$ [(e)–(h)]. Units: states eV^{-1} (formula unit)$^{-1}$.

IV. ANGLE-RESOLVED PHOTOELECTRON SPECTROSCOPY

Photoemission experiments have been performed in our home laboratory and at the Synchrotron Radiation Source in Daresbury (U.K.). At the Synchrotron we made use of the possibility to vary the photon energy continuously between 20 and 50 eV. In our home laboratory unpolarized light is obtained from a windowless differen- tially pumped gas discharge lamp which supplies light of 21.2 eV (He I) or 16.8 eV (Ne I). In both laboratories an ADES 400 spectrometer (Vacuum Generators) was used.

Single-crystalline platelets of $SnTaS_2$ were glued to the sample holder with silver-bearing resin. In both spectrometers the crystals were cleaved in the preparation chamber at a pressure of less than 10^{-8} torr, by stripping off a piece of tape stuck over it, to produce a fresh surface. The samples were immediately transported to the main chamber ($p \leq 10^{-10}$ torr) where they were examined by low-energy electron diffraction (LEED). A regular hexagonal pattern of sharp spots was observed, which allowed the azimuthal orientation of the samples with an accuracy of about 1°.

The only other angle-resolved photoemission studies of intercalates we are aware of are those by Hughes and coworkers, who studied the $3d$ transition-metal intercalates of TaS_2 (Refs. 20 and 21) and Ag_xTiS_2 (Ref. 22). They obtained peak widths comparable with our results for $SnTaS_2$, while angle-resolved ultraviolet photoelectron spectroscopy (ARUPS) measurements on nonintercalated layer compounds give much sharper peaks.[13] The surface of nonintercalated layered compounds consists only of chalcogen atoms, since the crystals are cleaved in the van der Waals gap. These surfaces are very stable and remain clean under UHV conditions for many days.[13,23] Intercalated materials are also cleaved in the van der Waals gap. Although very sharp LEED patterns are observed, there probably is a certain amount of surface roughness leading to broader peaks. After 48 h the quality of the surface was somewhat deteriorated as could be concluded from the increased amount of secondary electrons.

The measured energy-distribution curves are converted to E versus $\mathbf{k}_\parallel$ diagrams using the relation[24] $|\mathbf{k}_\parallel| = (2mE_{\rm kin})^{1/2}\sin\theta/\hbar$, where E is the initial state energy, $E_{\rm kin}$ the kinetic energy of the emitted electron, $\mathbf{k}_\parallel$ the photoelectron wave vector parallel to the surface, and θ the polar angle of emission of the electron.

Figure 10 shows He I spectra of $SnTaS_2$, when the polar angle θ is varied in the ΓKHA plane. The angle of incidence of the radiation α is 45°. The observed peak positions show only a small change in binding energy when θ is varied. Similar measurements, carried out with Ne I radiation of 16.8 eV, give the same peak positions. Measurements with negative θ give identical peak positions. We also measured spectra in the other high-symmetry plane ΓMLA with He I and Ne I radiation.

The measured binding energies of $SnTaS_2$ are compared with the results of the ASW band-structure calculations in Fig. 11. Solid circles represent peak positions

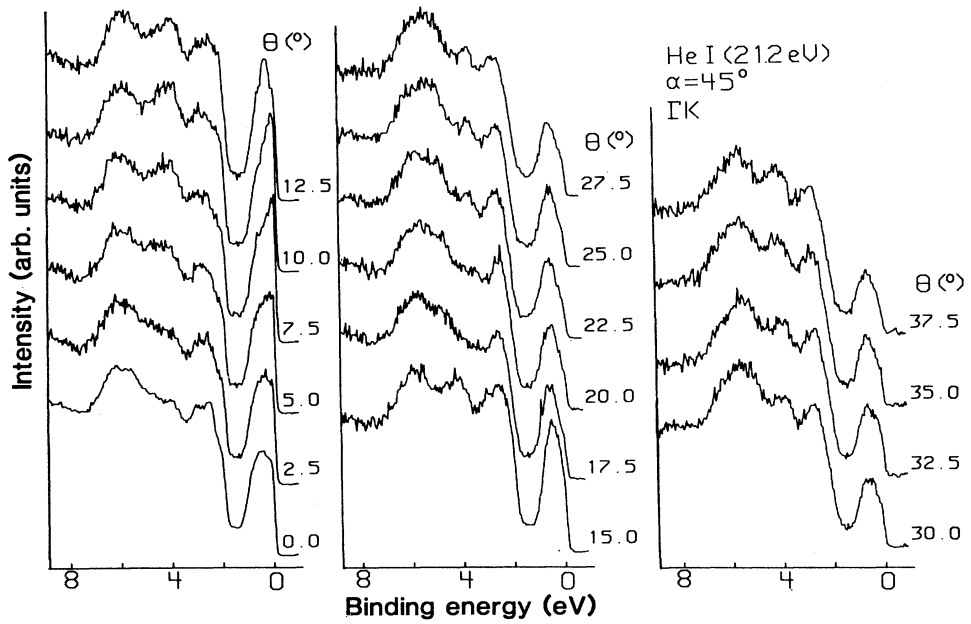

FIG. 10. He I ARUPS spectra of $SnTaS_2$ with $\alpha = 45°$ for emission at different angles θ in the ΓKHA plane.

and open circles shoulders in the spectra. In order to take into account the uncertainty in $\mathbf{k}_\perp$, the component of the wave vector normal to the surface, the calculated band structure is projected onto the surface Brillouin zone. In the surface Brillouin zone we then find regions, shaded in Fig. 11, in which the photoemission peaks should fall, irrespective of the exact nature of the photoemission process (direct or indirect transitions), under the condition that $\mathbf{k}_\parallel$ is a conserved quantum number. The energy width of these regions is a consequence of the uncertainty in $\mathbf{k}_\perp$ and the dispersion of the electron states in the normal direction. A reasonable agreement can be obtained when in the calculated band structure the Fermi level is shifted downward by 0.4 eV. Since the Fermi level lies in an energy range of very low density of states such a shift can already be caused by a slight tin deficiency in the sample or at the surface.

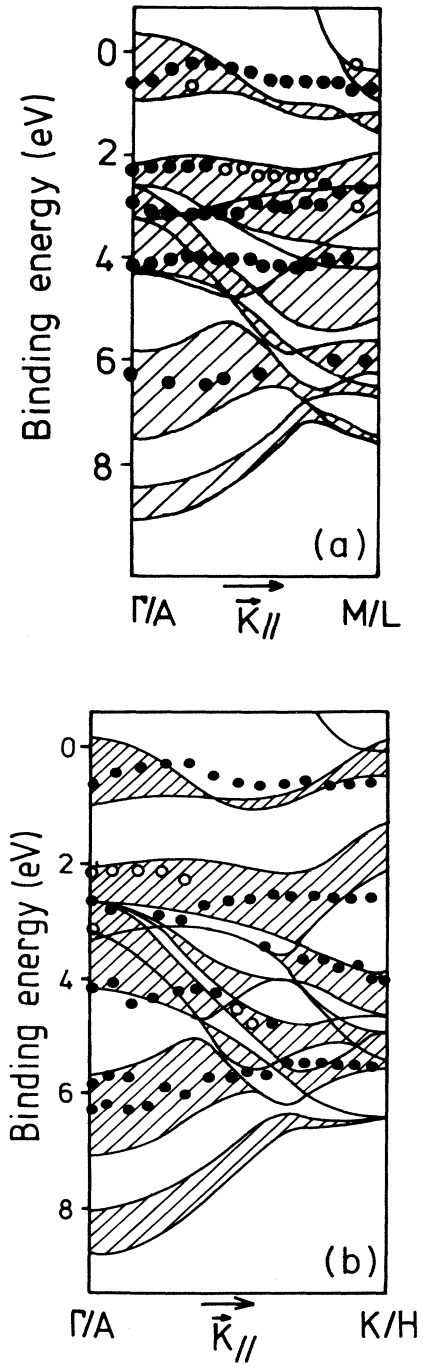

FIG. 11. Comparison of experimental and calculated band structure of $SnTaS_2$ in the (a) ΓMLA plane and (b) the ΓKHA plane.

The lowest band around 9 eV binding energy is almost completely of Sn 5*s* character. Since the cross sections of the Sn 5*s* and 5*p* states are very low[25] these states are not observed in the spectra. The uppermost band can be identified as the Ta d_{z^2} band, while the lower lying peaks between 2 and 7 eV binding energy are S 3*p* states. Not all the calculated bands are resolved in this region; the peaks are too wide. The total width of the S 3*p* band (without Sn 5*s*) is in agreement with the calculations. The measured Ta 5*d*–S 3*p* peak-to-peak distance of 1.5 eV is equal to the value found in the calculation. The Ta d_{z^2} band shows up in the spectra as a very asymmetric peak, present very clearly everywhere in the Brillouin zone, which proves the increased filling of the Ta d_{z^2} band by intercalation. The observed dispersion of the Ta d_{z^2} band is somewhat smaller than calculated. The highest intensity is reached when $\theta = 12.5° - 15°$, i.e., when the peak position is closest to the Fermi level.

The valence-band structure of $SnTaS_2$ was also studied by photon-energy-dependent photoelectron spectroscopy, using the Synchrotron Radiation Source in Daresbury. Figure 12 shows the normal emission ($\theta = 0°$) energy-distribution curves recorded as a function of the energy of the incoming radiation. Peak positions of the different spectra show only small energy shifts. This can have two causes. (1) The photoemission process is a direct transition, but the bands show only a small dispersion in the normal direction; (2) the photoemission is due to indirect transitions and the spectra show more or less a one-dimensional density of states.

One can distinguish between the direct and indirect transition model for the photoemission process on basis of the ratio l/c of the effective electron mean free path l and the interplanar distance normal to the surface, c. When $l/c \gg 1$ direct transitions prevail in the spectra. In the case of $l/c < 1$ the uncertainty in k_z is of the order of the dimension of the Brillouin zone in the z direction and the spectra are determined by the extrema in the one-dimensional density of states along a particular line in the k_z direction. For photon energies smaller than 50 eV l is between 5 and 15 Å, while c is 8.7 Å per slab in the case of $SnTaS_2$. The spectra of Fig. 12 were all taken at $\theta = 0°$, so that we are looking along ΓA in the Brillouin zone. We find that the measured peak positions do not correspond to the extrema in the one-dimensional density of states, calculated with the ASW method.

In the direct transition model the determination of the exact peak positions requires a knowledge of the dispersion of the final state. In most cases a free-electron final state is used, but from the small energy shifts observed in

our normal emission spectra it is clear that such an approach is not useful in this case. We conclude that it is not possible from our measurements to discern clearly between the direct or the indirect transition model; probably both types of transitions contribute in $SnTaS_2$.

From the spectra of Fig. 12 more information can be abstracted by analyzing the photon-energy dependency of the peak intensities. This gives information about the atomic character of the initial states. In Fig. 13 the intensities of the four most pronounced peaks in the spectra, relative to the intensity of the lowest S $3p$ band around 6 eV binding energy, are shown. The Ta $5d$ cross section increases compared to that of the S $3p$ states with increasing photon energy.[25] Further, the intensity of the Ta $5d$ states shows a resonantlike behavior around 25 eV due to the interference with the Ta $4f$-$5d$ Coster-Kronig Auger decay. The intensity of the Ta d_{z^2} band just below the Fermi level is suppressed at a photon energy of about 25 eV—the binding energy of the Ta $4f$ core electrons—and increases strongly for higher photon energies. Therefore the peaks with the strongest enhancement of intensity with increasing photon energy have the largest amount of Ta $5d$ character. From Fig. 13 we see the strongest increase for the highest band, the Ta d_{z^2} band. The two peaks at 2.3 and 2.9 eV binding energy also increase in intensity compared with the lowest band, which means that there is a considerable amount of Ta $5d$ character covalently mixed in these S $3p$ states. The lowest band, the reference state in Fig. 13, decreases in intensity with higher photon energies and is thus mainly composed of S $3p$ wave functions. The band-structure

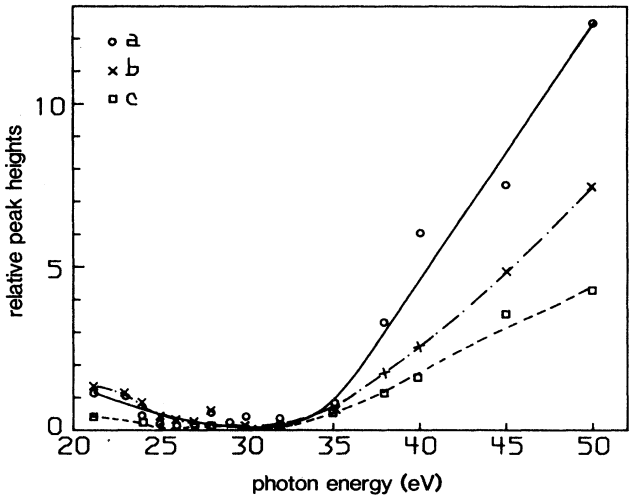

FIG. 13. Intensity (peak height) as a function of photon energy of the main peaks in the normal emission spectra of $SnTaS_2$, relative to the intensity of the lowest-lying S $3p$ peak at 6 eV binding energy. (a) Peak at binding energy 1 eV (Ta $5d_{z^2}$); (b) peak at binding energy 2.3 eV; (c) peak at binding energy 2.9 eV.

calculations indicate that this band originates from S $3p_z$ states, while the bands between 2 and 3 eV consist of S $3p_xp_y$ functions, strongly hybridized with Ta $5d_{xy}$ and $5d_{x^2-y^2}$.

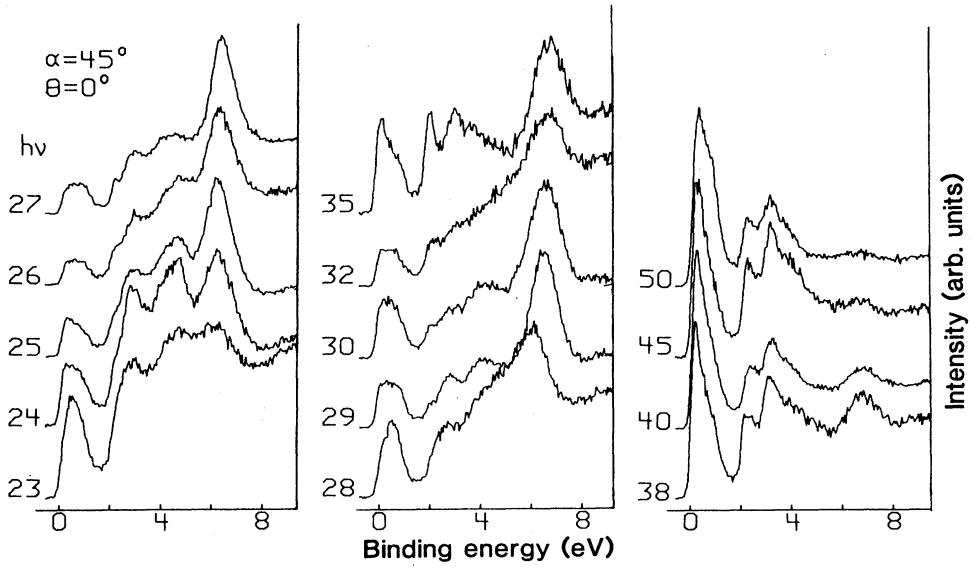

FIG. 12. Energy-distribution curves of $SnTaS_2$ at the Γ point of the surface Brillouin zone ($\theta=0°$) with photon energies between 23 and 50 eV.

V. EXPERIMENTAL RESULTS OF PHYSICAL PROPERTIES OF $SnTaS_2$

The electrical resistivity, Hall effect, and thermoelectric power of the intercalation compounds M_xTX_2 (M=Sn,Pb; T=Nb,Ta; X=S,Se; $x=\frac{1}{3},1$) were reported by Eppinga *et al.*[7] These intercalation compounds all show good metallic conductivity. In this section we report some new and more accurate data on single-crystalline platelets of $SnTaS_2$.

Figure 14 shows the electrical resistivity of $SnTaS_2$ as a function of temperature. The residual resistivity $\rho(T=0)=2.5\times10^{-9}$ Ω m is quite small, indicating small atomic disorder and small concentration of defects in the crystal.

On the same single-crystalline platelet the Hall effect was measured in the temperature range between 4.2 and 300 K with magnetic fields perpendicular to the crystal plate, varying from −3 to +3 T. R_H is positive over the whole temperature range (see Fig. 15), indicating that the charge carriers are effectively holelike, in agreement with the calculated Fermi surface of the Sn $5p_xp_y$ band (Fig. 7). The decrease of R_H with temperature from 8×10^{-10} m^3/C at low temperature to 3×10^{-10} m^3/C at room temperature can be due to the presence of two types of charge carriers.

The thermoelectric power (or Seebeck coefficient) α of $SnTaS_2$ was measured in the temperature range from 4.2 to 330 K (Fig. 16). The peak at 29 K is probably caused by the phonon drag. The thermoelectric power of metals (without the phonon-drag contribution) can be written as[26]

$$\alpha=-\frac{\pi^2k^2T}{3e}\left[\frac{\partial\ln\Lambda}{\partial E}+\frac{\partial\ln S}{\partial E}\right]_{E=E_F},$$

where Λ is the mean free path of the charge carriers and S is the Fermi-surface area. The thermopower α is positive, i.e., it has the sign for hole conduction. A positive sign of α indicates that the Fermi surface S shrinks with increasing energy. Such a shrinking of the Fermi surface with increasing energy is the behavior expected for the Fermi surface coming from the Sn $5p_xp_y$ bands. The fact that both the thermopower and the Hall effect are positive indicates that the two-dimensional Sn $5p_xp_y$ bands are mainly responsible for the electrical properties, while the small electron pockets at H only play a minor role. Previously published measurements[6,7] are essentially in agreement with ours.

$SnTaS_2$ and $PbTaS_2$ are superconducting below 2.75 and 1.7 K, respectively.[5] In order to obtain more information about the superconductivity of these highly two-dimensional metals, we measured the low-temperature specific heat C of a pressed powder sample of $SnTaS_2$ between 1.4 and 10 K. The data show a sharp anomaly at 2.8 K, which disappeared when a magnetic field of 1 T was applied (Fig. 17). The strong dependence on magnetic field indicates that below a critical temperature

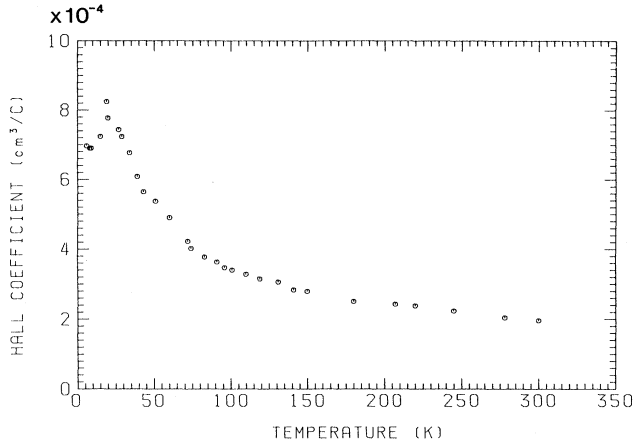

FIG. 15. Hall coefficient R_H of $SnTaS_2$, measured with the magnetic field perpendicular to the *ab* plane.

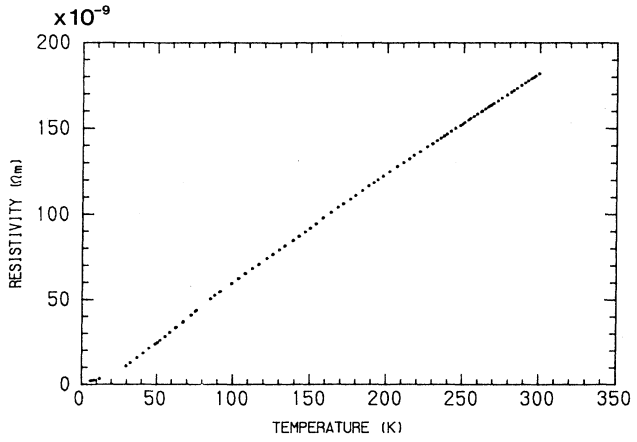

FIG. 14. Specific resistivity ρ of $SnTaS_2$, measured in the *ab* plane.

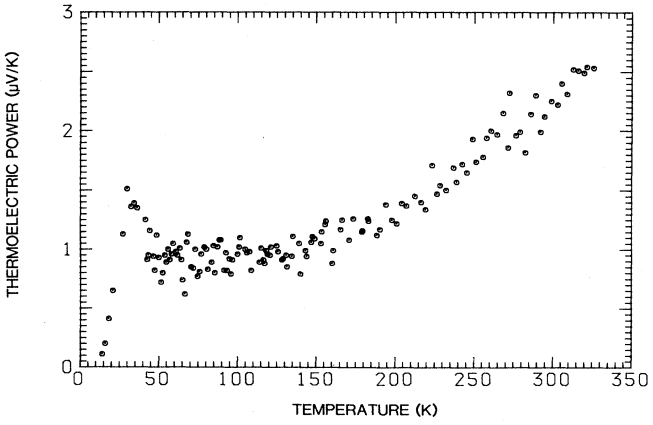

FIG. 16. Thermoelectric power α of $SnTaS_2$, measured in the direction perpendicular to the *ab* plane.

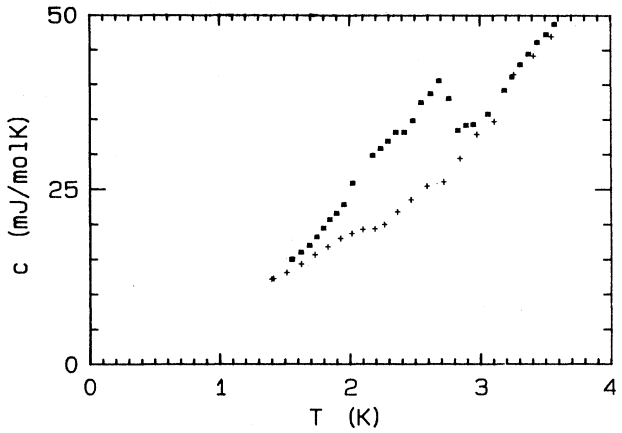

FIG. 17. Specific heat C of $SnTaS_2$ without magnetic field (squares) and in the presence of an applied magnetic field of 1 T (crosses).

$T_C = 2.8$ K $SnTaS_2$ is superconducting.

The heat-capacity anomaly at 2.8 K amounts to $\Delta C/T_C = 4.6\times10^{-3}$ J/mol K^2, where ΔC is the difference in heat capacity between the superconducting state and the normal state. Using the value of the electronic contribution to the specific heat (7.0×10^{-3} J/mol K^2, see below), we find $\Delta C/\gamma T_C \approx 0.7$, appreciably smaller than the standard BCS value of 1.43.

Apart from the heat-capacity anomaly due to superconductivity, the specific heat is usually written as the sum of an electronic contribution γT and a phonon contribution βT^3. The coefficients γ and β are then obtained by plotting C/T versus T^2. The observed data of $SnTaS_2$ follow this $C=\gamma T+\beta T^3$ behavior only in a very restricted temperature range (see Fig. 18). A least-squares fit between T_C and 4.5 K gives the values $\gamma = 7.0\times10^{-3}$ J/mol K^2 and $\beta = 5.3\times10^{-4}$ J/mol K^4. Above 4.5 K a strong deviation from the normal behavior is observed: C increases stronger with increasing temperature than the T^3 law expected for harmonic vibrations. In fact, C is proportional to $T^{7/2}$ in a large temperature range (3–10 K). Such a more rapid increase of C with T is expected for compounds with strongly anharmonic vibrations. A large anharmonicity is also consistent with the very large and anisotropic vibrational amplitude of Sn atoms at room temperature as observed with Mössbauer spectroscopy.[27]

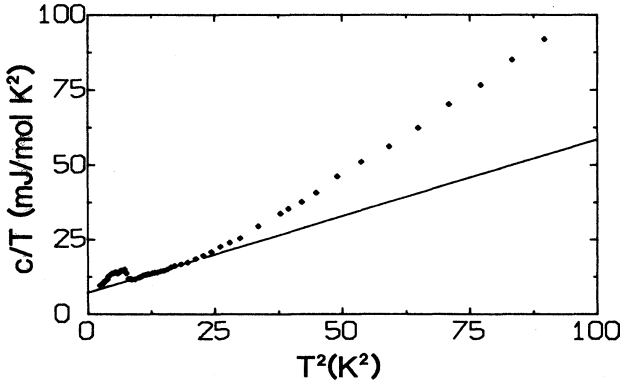

FIG. 18. C/T vs T^2 of $SnTaS_2$.

From the value of γ and the density of states at the Fermi level $N(E_F)$ it is possible to calculate the electron-phonon coupling constant λ, using the relation $\gamma=(1+\lambda)(2\pi^2k_B^2/3)N(E_F)$. With the value of $N(E_F)$ from the band-structure calculation we obtain $\lambda=0.5$. Under the assumption that the transport properties are only determined by the Sn $5p_xp_y$ band, one would calculate for λ a value of 1.9, since the Sn $5p_xp_y$ contribution to $N(E_F)$ is about 50%. Using the relation $\beta=1944/\Theta_D^3$, a value for the Debye temperature Θ_D of 154 K is calculated, in agreement with the value of 176 K obtained from Mössbauer data.[27] We remark that the values of γ and β (and also the λ value) are inaccurate, as they were obtained from a fit of C/T versus T^2 in a very restricted temperature range.

The two-dimensional character of the Sn $5p_xp_y$ conduction electrons and/or holes in $SnTaS_2$ is also observed in NMR measurements.[28] The ^{119}Sn Knight shift of $SnTaS_2$ is very anisotropic, in contrast with $Sn_{1/3}TaS_2$, where the Sn Knight shift is completely isotropic due to the octahedral coordination of Sn. The value of the Sn Knight shift in $SnTaS_2$ is about the same as found for α-Sn and much larger than for typical Sn^{2+} compounds, indicating a considerable Sn conduction-electron density of states at E_F. That the Sn atoms have a valency less than 2 is also clear from the isomershifts measured by Mössbauer spectroscopy.[27] The Sn isomer shift in $SnTaS_2$ is 3.13 mm/s with respect to $BaSnO_3$. This value for $SnTaS_2$ is in between the values found for α-Sn (2.53 mm/s) and for Sn^{2+} in $Sn_{1/3}TaS_2$ (3.85 mm/s).

Also some spectroscopic studies of post-transition-metal intercalates have been published. The rigid-band model for this class of compounds is confirmed by x-ray absorption[29] and valence-band x-ray photoemission spectroscopy.[7,8] The $4f$ core lines of Ta in $2H$-TaS_2 and $Sn_{1/3}TaS_2$ show asymmetric broadening at the high-binding-energy side, which is a consequence of the Ta partial density of states at E_F. The asymmetry decreases with increasing Sn content, since filling up the Ta d_{z^2} band leads to a smaller Ta partial DOS at the Fermi level. For $SnTaS_2$ the Ta core levels are symmetric, indicating that the Ta d_{z^2} band is completely filled.

VI. Sn 4*d* CORE-LEVEL SPECTROSCOPY

The Sn $5s$ and $5p$ valence states were not observed with ARUPS, because of their low cross section. However, the valence state of the intercalated tin atoms can be studied with core-level spectroscopy. Eppinga *et al.*[8] measured the Sn $3d$ core levels of $SnTaS_2$ and $Sn_{1/3}TaS_2$. For $Sn_{1/3}TaS_2$ they found a single Sn $3d^{5/2}$ line at a bind-

ing energy corresponding with a formal valency of 2^+ for the Sn ion. The Sn $3d^{5/2}$ level of $SnTaS_2$ showed a splitting into two components with equal intensity and an energy difference of 1.0 eV. It was shown that a gradual removal of the top layers by bombardment with 800-eV argon ions did not alter the spectra: the width, splitting and intensity ratio of the two components of the Sn $3d$ spectra remained unchanged. This indicates that the spectra are due to bulk Sn atoms; if one of the components were due to surface Sn atoms, one would expect its intensity to decrease more rapidly under ion bombardment. On the basis of these data Eppinga *et al.*[8] suggested that the presence of two peaks in the spectrum is caused by Sn atoms with two different valencies, arising from a valence disproportionation

$$2\ Sn^+(5s^25p^1) \rightarrow Sn^0(5s^25p^2) + Sn^{2+}(5s^2)\ .$$

Because there is only one Sn position in the crystal structure of $SnTaS_2$, the presence of two valencies must be accompanied by a rapid valence fluctuation $Sn^0 + Sn^{2+} \leftrightarrow Sn^{2+} + Sn^0$. A similar splitting was observed for the Pb $4f$ core levels in $PbTaS_2$ and $PbNbS_2$,[8] indicating a valence disproportionation $2\ Pb^+(6s^26p^1) \rightarrow Pb^0(6s^26p^2) + Pb^{2+}(6s^2)$ and valence fluctuations $Pb^0 + Pb^{2+} \leftrightarrow Pb^{2+} + Pb^0$. It was also pointed out that for sufficiently rapid valence fluctuations one will not observe two types of Sn atoms with Mössbauer or NMR, but rather a single signal with parameters which are the average of the two types of Sn atoms. With photoelectron spectroscopy two types of Sn atoms can be observed, since the time scale of photoelectron spectroscopy ($\sim 10^{-15}$ sec) is much shorter than of Mössbauer or NMR.

We measured the Sn $4d$ core levels with synchrotron radiation using photon energies of 45 and 70 eV. The Sn $4d$ core-level binding energies are in the same binding-energy region as the Ta $4f$ states, around 25 eV, but due to cross-section effects they can be well separated. For XPS, using Al $K\alpha$ radiation of 1486.6 eV, the cross section of Sn $4d$ is about 30% of that of Ta $4f$,[25] which partly explains that no Sn $4d$ levels are distinguished in the Ta $4f$ spectra of Eppinga.[8] The calculated cross section of Sn $4d$ is about 20 times the cross section of Ta $4f$ for a photon energy of 70 eV and even larger at 45 eV.[25] In Figs. 19(a) and 19(b) the Sn $4d$–Ta $4f$ core-level spectra are shown. They consist of three large peaks at 24.3, 25.3, and 26.4 eV binding energy and a smaller one at 23.0 eV. From comparison with the Ta $4f$ binding energies,[30] it can be concluded that the small peak at 23.0 eV is the Ta $4f^{7/2}$ peak. The other three peaks come from Sn $4d$, overwhelming the underlying Ta $4f^{5/2}$. It is possible to fit the 70-eV photon-energy spectrum, after background correction, with two $d^{5/2}$-$d^{3/2}$ doublets with equal intensity and a relative energy shift of 1.03 eV, under the assumption that the intensities of the $\frac{5}{2}$ and $\frac{3}{2}$ peaks are in the proportion of 3:2 [see Fig. 19(c)]. So it seems that two types of Sn atoms are observed with the following binding energies: $Sn^a\ 4d^{3/2}$ (26.39 eV), $Sn^a\ 4d^{5/2}$ (25.34 eV), $Sn^b\ 4d^{3/2}$ (25.36 eV), $Sn^b\ 4d^{5/2}$ (24.31 eV). The spin-orbit splitting of 1.05 eV of our fit is in agreement with the known atomic value.

It is more difficult to make a reliable fit of the Sn $4d$ core levels of the spectrum taken with 45-eV photon energy, because the peaks are situated in a kinetic energy

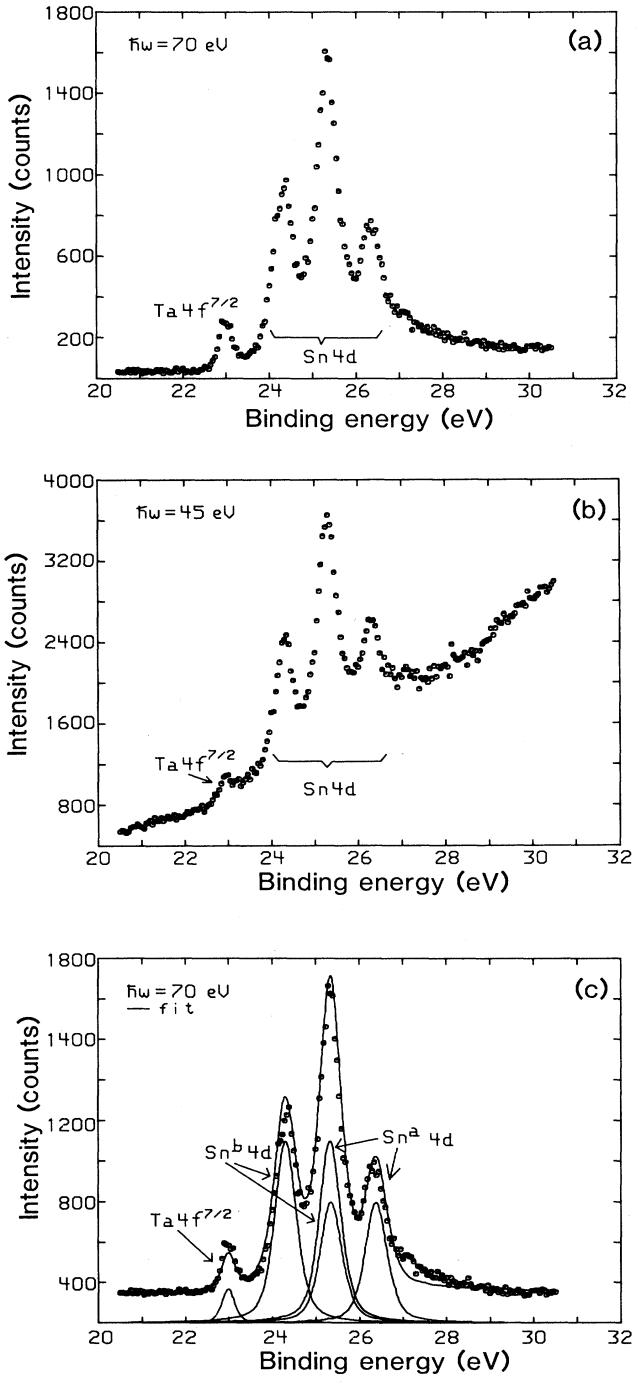

FIG. 19. Sn $4d$ core-level spectra of $SnTaS_2$ at room temperature with photon energies (a) of 70 eV and (b) 45 eV. The four-component fit of the 70-eV spectrum, explained in the text, is shown in (c).

region with a strongly increasing intensity of secondary electrons. However, the number of peaks and their separation are the same as found in the 70-eV spectrum, while their relative intensities are also the same.

In order to determine whether we are measuring bulk or surface properties, an estimate is made of the escape depth l of the Sn core electrons in the different spectra. Using the universal curve of l versus the kinetic energy of the photoelectrons[31] the escape depth of electrons excited by 1486.6 eV from the Sn 3*d* core levels is about 20 Å, the value for electrons excited with 45 or 70 eV photons from the Sn 4*d* levels is about 10 Å. Nevertheless, the relative intensity of the two types of Sn atoms is the same in all these cases (45, 70, and 1486 eV photon energy). This indicates that the peak splitting is an intrinsic bulk effect. It was already suggested by Eppinga *et al.*[7,8] that the formally monovalent Sn atoms are rapidly fluctuating between Sn^{2+} and Sn^{0}. A similar charge disproportionation is frequently observed in post-transition-metal compounds[32] where the post-transition-metal ions have an uncommon formal valency. Examples are TlSe ($Tl^{1+}Tl^{3+}2\ Se^{2-}$), Pb_3O_4 ($2\ Pb^{2+}Pb^{4+}4\ O^{2-}$), and $CsSbCl_5$ ($2\ Cs^{1+}Sb^{3+}Sb^{5+}10\ Cl^{1-}$). However, in all these cases the charge disproportionation is clearly visible in the crystal structure, in which there are two inequivalent lattice sites with a different coordination of post-transition-metal ions by anions. In $SnTaS_2$ all Sn atoms are (on the average) equivalent. $SnTaS_2$ is comparable with the pyrazide-bridged Ru(II,III) ammine complex, where the time scale of the experiment is also decisive for the observed valencies.[32,33]

Mössbauer measurements[27] show a very large anisotropy in the vibration amplitude of the tin atoms at room temperature. The vibration amplitude in the direction of the c axis is much smaller than in the ab plane: $\langle x_{\perp c}\rangle^2-\langle x_{\parallel c}\rangle^2=(0.22)^2$ Å^2. This anisotropy is not unexpected for such a loose packing of the atoms in the intercalant layers. The position with the linear coordination does not seem to be very stable, indicating that the existence of this compound is more a consequence of the in-plane metal-metal interaction than of the Sn $5p_z$–S $3p_z$ hybridization. One expects a strong coupling of the large vibrations at room temperature of the Sn atoms in the ab plane with the charge disproportionation observed by photoelectron spectroscopy. Generally, there is a tendency for Sn^{1+} ions to disproportionate into Sn^{0} and Sn^{2+}, and these two types of Sn atoms will prefer different types of coordination by S atoms. However, the TaS_2 host lattice is very rigid. The a axis hardly changes during intercalation with different types of atoms, which indicates that the host lattice is too rigid to be strongly changed by the possible charge disproportionation of Sn. Therefore, the change of valency can easily induce a shift of the Sn atoms, and a fluctuating valence will correspond to large vibrational amplitudes of Sn.

In order to see whether a static change in position of half of the tin atoms in one plane would be accompanied by a charge redistribution between them, we have performed band-structure calculations on fictive $SnTaS_2$ in which two different positions in the intercalant layer are created in the following way. The unit cell of 1*s*-$SnTaS_2$ is doubled in the ab plane. Of the two tin atoms in the unit cell one, called Sn(2), is shifted away from its linearly coordinated position, while the other—Sn(1)—is fixed at the linearly coordinated position. Calculations have been performed for different directions and distances of this displacement. It is found that the charge redistribution is nearly independent of the direction of the displacement of the Sn(2) in the ab plane. The dependence on the magnitude of the displacement was determined by shifting the Sn(2) atoms along the a axis. When shifted over the maximum amount of $a/2$ (1.65 Å) the difference of the charge density within the equally sized Wigner-Seitz spheres of the two types of Sn atoms is 0.09 electron. The difference between the two types of Sn atoms is most clearly observed in the calculated core-level binding energies, which show a chemical shift. The relative chemical shift of the Sn 4*d* core levels reaches a maximum value of 0.64 eV, when the displacement of the Sn(2) is $a/2$ (1.65 Å). This is of the same order as the chemical shift of 1.03 eV observed in the photoemission (3*d* and 4*d* core peaks). The larger binding energy is found for the Sn(2) atom which is shifted away from the linear coordinated position. This means that the shifted atom is more electropositive than the fixed, linearly coordinated Sn(1).

VII. CONCLUSIONS

Band-structure calculations of $SnTaS_2$ and related intercalates show that for post-transition-metal intercalates of TaS_2 the rigid-band model is a reasonable first-order approximation. Only small changes occur in the TaS_2 partial band structure, while the Ta $5d_{z^2}$ band is filled up with electrons donated by the intercalant atoms. For fully intercalated $SnTaS_2$ the Ta $5d_{z^2}$ band is completely filled. The Fermi level is crossed by the Sn $5p_xp_y$ band and by one Ta d band. The Fermi surface coming from the Sn $5p_xp_y$ consists of rosette-shaped parallel rods along the c axis. Small electron pockets are present around H.

Calculated band structures of $PbTaS_2$ and $GeTaS_2$ are much the same as of $SnTaS_2$. Only the intercalant p_xp_y bands have a different width and the Fermi level is only crossed by the intercalant p_xp_y band. In $GeTaS_2$ and $PbTaS_2$ the lowest energy of the (non-d_{z^2}) Ta 5*d* band is positioned in H, as in the case of $SnTaS_2$, but the eigenvalue in H just lies above E_F.

The positive sign of the thermoelectric power as well as the Hall effect of $SnTaS_2$ indicates that the transport properties are mainly determined by the Sn $5p_xp_y$ band. $SnTaS_2$ is superconducting below $T_C=2.8$ K, as shown by resistivity and specific-heat measurements.

The stabilization of 1*s*- and 2*s*-$SnTaS_2$ has three causes: (1) the charge transfer of one electron from Sn 5*p* to the Ta d_{z^2} band, (2) the Sn-S covalency in the c direction, and (3) the overlap of the in-plane Sn $5p_xp_y$ orbitals. This overlap leads to a 10.9-eV-wide Sn $5p_xp_y$ band, which is occupied by one electron. The fact that a similar Ge $4p_xp_y$ band in $GeTaS_2$ has a much smaller width is probably the reason for the nonexistence of this compound. Calculations of fictive $SnTaS_2$ with the Sn atoms in other

coordinations by the sulfur atoms and shorter Sn-Ta distances, show stronger Sn-Ta interactions, which disturb the formation of the two-dimensional Sn $5p_xp_y$ band. The rigid-band model is no longer a good approximation, when intercalant-host interactions are increased.

ARUPS measurements sustain the calculated band structure. The Sn 4*d* core levels show a clear splitting of 1 eV, which is interpreted as a consequence of the instability of the $Sn^{1+}(5s^25p^1)$ ions. Coupled with a large vibration amplitude of the Sn atoms in the *ab* plane is a valence disproportionation $2\,Sn^{1+} \rightarrow Sn^{2+} + Sn^0$, concomitant with rapid valence fluctuations $Sn^0 + Sn^{2+} \leftrightarrow Sn^{2+} + Sn^0$.

ACKNOWLEDGMENTS

We would like to extend our thanks to R. Coehoorn, C. F. J. Flipse, D. Norman, D. Law, and A. Heeres for their assistance during the photoelectron spectroscopy experiments. One of us (R. A. de G.) wants to thank the Stichting voor Fundamenteel Onderzoek der Materie (FOM) for financial support.

*Present address: Philips Research Laboratories, P.O. Box 80 000, 5600 JA Eindhoven, The Netherlands.

[1]G. V. Subba Rao and M. W. Shafer, in *Physics and Chemistry of Layered Materials,* Vol. 6 of *Intercalated Layered Materials,* edited by F. Levy (Reidel, Dordrecht, 1979), p. 99.
[2]R. H. Friend and A. D. Yoffe, Adv. Phys. **36**, 1 (1987).
[3]A. R. Beal, in Ref. 1, p. 251.
[4]J. Rouxel, in Ref. 1, p. 201.
[5]F. J. Di Salvo, G. W. Hull, Jr., L. H. Schwartz, J. M. Voorhoeve, and J. V. Waszcak, J. Chem. Phys. **59**, 1922 (1973).
[6]R. Eppinga and G. A. Wiegers, Physica B+C **99B**, 121 (1980).
[7]R. Eppinga, G. A. Wiegers, and C. Haas, Physica B+C **105B**, 174 (1981).
[8]R. Eppinga, G. A. Sawatzky, C. Haas, and C. F. van Bruggen, J. Phys. C **9**, 3371 (1975).
[9]G. Y. Guo and W. Y. Liang, J. Phys. C **20**, 4315 (1987).
[10]A. R. Williams, J. Kübler, and C. D. Gelatt, Jr., Phys. Rev. B **19**, 6094 (1979).
[11]L. Hedin and B. I. Lundquist, J. Phys. C **4**, 2064 (1971).
[12]M. Methfessel and J. Kübler, J. Phys. F **12**, 141 (1982).
[13]R. Coehoorn, C. Haas, J. Dijkstra, C. F. J. Flipse, R. A. de Groot, and A. Wold, Phys. Rev. B **35**, 6195 (1987).
[14]R. Huisman, R. de Jonge, C. Haas, and F. Jellinek, J. Solid State Chem. **3**, 56 (1971).
[15]L. F. Mattheis, Phys. Rev. Lett. **30**, 784 (1973); Phys. Rev. B **8**, 3719 (1973).
[16]R. Coehoorn, A. A. van Heuzen, C. Haas and G. A. Sawatzky, in *Festkörperprobleme (Advances in Solid State Physics),* edited by P. Grosse (Vieweg, Braunschweig, 1985), Vol. XXV, p. 459.
[17]F. R. Shepherd and P. M. Williams, J. Phys. C **7**, 4427 (1974).
[18]R. Eppinga and G. A. Wiegers, Mater. Res. Bull. **12**, 1057 (1977).
[19]J. Dijkstra, Ph.D. thesis, University of Groningen, 1988.
[20]J. J. Barry and H. P. Hughes, J. Phys. C **15**, 1797 (1982).
[21]J. J. Barry and H. P. Hughes, J. Phys. C **16**, 5393 (1983).
[22]H. I. Starnberg and H. P. Hughes, J. Phys. C **20**, 4429 (1987).
[23]F. Minami, M. Sekita, N. Aono, and N. Tsuda, Solid State Commun. **29**, 459 (1979).
[24]F. J. Himpsel, Adv. Phys. **32**, 1 (1983).
[25]J. J. Yeh and I. Lindau, Atom. Data Nucl. Data Tables **32**, 1 (1985).
[26]R. D. Barnard, *Thermoelectricity in Metals and Alloys* (Taylor and Francis, London, 1972).
[27]R. H. Herber and R. F. Davis, J. Chem. Phys. **63**, 3668 (1975); **65**, 3773 (1975); J. Solid State Chem. **27**, 137 (1979); R. H. Herber, F. J. Di Salvo, and R. B. Frankel, Inorg. Chem. **19**, 3135 (1980); R. H. Herber, Acc. Chem. Res. **15**, 216 (1982); R. H. Herber and H. Eckert, in *Chemical Mössbauer Spectroscopy,* edited by R. H. Herber (Plenum, New York, 1985), p. 133.
[28]A. C. Gossard, F. J. Di Salvo, and H. Yasuoka, Phys. Rev. B **9**, 3965 (1974).
[29]Y. Ohno, K. Kaneda and K. Hirama, Phys. Rev. B **30**, 4648 (1984).
[30]J. Folmer and D. K. G. de Boer, Solid State Commun. **38**, 1135 (1981).
[31]I. Lindau and W. E. Spicer, J. Electron Spectrosc. **3**, 409 (1974).
[32]P. Day, Int. Rev. Phys. Chem. **1**, 149 (1981).
[33]C. Creutz and H. Taube, J. Amer. Chem. Soc. **95**, 1086 (1973).